INTERNATIONAL JOURNAL OF CLIMATOLOGY
Int. J. Climatol. (2017)
Published online in Wiley Online Library
(wileyonlinelibrary.com) DOI: 10.1002/joc.5232

RMetS
Royal Meteorological Society

Evaluation of regional COSMO-CLM climate simulations over the Eastern Mediterranean for the period 1979–2011

Assaf Hochman,[a,b]* Edoardo Bucchignani,[c,d] Giora Gershtein,[e] Simon O. Krichak,[a] Pinhas Alpert,[a] Yoav Levi,[e] Yizhak Yosef,[a,e] Yizhak Carmona,[e] Joseph Breitgand,[a] Paola Mercogliano[c,d] and Alessandra L. Zollo[c,d]

[a] *Department of Geosciences, School of Geosciences, Tel Aviv University, Israel*
[b] *Porter School of Environmental Studies, School of Geosciences, Tel-Aviv University, Israel*
[c] *CMCC Euro-Mediterranean Center on Climate Change, Impacts on Soil and Coast Division, Capua, Italy*
[d] *Meteorology Lab, CIRA Centro Italiano Ricerche Aerospaziali, Capua, Italy*
[e] *Research, Israel Meteorological Service, Beit-Dagan, Israel*

ABSTRACT: The Regional Climate Model (RCM) COSMO-CLM capability to reproduce the climate characteristics, including extreme values, over the Eastern Mediterranean (EM) was tested. Model configuration has been chosen based on a previously performed sensitivity analysis, aimed to ascertain the accuracy of model performances over Israel. Three simulations driven by ERA Interim reanalysis data for 1979–2011 have been performed using the 0.44°, 0.22° and 0.0715° horizontal resolutions equivalent to about 50, 25 and 8 km, respectively. The CORDEX-MENA domain has been employed for the simulation at resolutions 0.44° and 0.22°. Nested in the 0.22° domain the highest resolution of 0.0715° is performed over Israel. The model response was analysed for daily precipitation, 2 m average temperature, maximum temperature, minimum temperature and a subset of climate indicators defined by the Expert Team on Climate Change Detection and Indices for temperature and precipitation. Results were inter-compared and evaluated against observations. The increased resolution was found to improve precipitation and temperature results. Extreme precipitation indices were well reproduced compared with observations, with a 13% averaged percentage bias. COSMO-CLM was able to reproduce the EM precipitation gradients, with mostly overestimations in the coastal plains and underestimations in the mountains. Extreme temperature indices related to maximum temperatures were reproduced relatively well with an averaged percentage bias of 5.7%. The ability of the model to reproduce minimum temperature observational values was found to be highly dependent on station location with respect to topography. The results in this study are considered a substantial improvement from earlier RCM evaluation studies.

KEY WORDS extreme precipitation; extreme temperature; COSMO-CLM; RCM; ETCCDI

Received 16 September 2016; Revised 12 July 2017; Accepted 12 July 2017

1. Introduction

Atmosphere Ocean Global Climate Models (AOGCM) are considered as a comprehensive tool for studying climate conditions. Still the resolution of contemporary AOGCMs is typically insufficient for the representation of smaller scale (mesoscale) processes determining climate conditions in the quite complex Mediterranean region (Lionello *et al.*, 2014). Application of Regional Climate Models (RCM) is usually necessary for providing information at a sufficient degree of detail (Laurent *et al.,* 2012). However, the added value of high-resolution simulations is not always evident (Chan *et al.,* 2013). The use of higher resolution RCMs does not always lead to an improvement of the model performance. Hence, it is not obvious whether the increase in spatial resolution will always provide a better representation of the climate in general and the extremes in particular.

It is standard practice to evaluate RCM configuration driven by reanalysis data archives, which may be considered as 'observations' before the model is adopted for downscaling of AOGCM past, present, or future runs (Toreti and Naveau, 2015). It has to be also noted that application of the strategy makes possible an evaluation of the ability of an RCM to reproduce not only the climate means but also the extremes, because climate extremes are by definition rare events, which are hard to predict (García-Cueto and Santillán-Soto, 2012).

An RCM with a specific setup configuration may be (and typically is) appropriate for representing climate conditions of a sub-region. In this respect, it must be noted that RCMs and their configurations are not the sole factors responsible for inaccuracies in the climate representation. The role of the processes affecting the climate of the region, as well as that of the accuracy of climate (or climate change) representation with Global Climate Models (GCM) outside the RCM domain must also be evaluated.

The adopted strategy of evaluation, in the current study, appears to be especially necessary for the simulation of climate in the Eastern part of the Mediterranean region (EM).

* Correspondence to: A. Hochman, Department of Geosciences, School of Geosciences, Tel Aviv Unversity, Tel Aviv 69978, Israel. E-mail: assafhochman@post.tau.ac.il; assafhochman@yahoo.com

Table 1. List of indicators considered for precipitation.

Label	Description	Units
SDII	Mean precipitation on wet days (>1 mm)	mm day^{-1}
CWD	Maximum number of consecutive wet days (>1 mm)	days year^{-1}
Rx1day	Maximum of daily precipitation	mm day^{-1}
R10	Number of days with precipitation ≥10 mm day^{-1}	days year^{-1}
R20	Number of days with precipitation ≥20 mm day^{-1}	days year^{-1}
99p	99th percentile of daily precipitation	mm day^{-1}
90p	90th percentile of daily precipitation	mm day^{-1}
CDD	Maximum number of consecutive dry days (<1 mm)	days year^{-1}

Table 2. List of indicators considered for temperature.

Label	Description	Units
SU	Summer days – annual count of days when the daily T_{max} is above 25°	days year^{-1}
90p Tmax	90th percentile of daily T_{max}	°C
TXx	Annual maximum value of daily T_{max}	°C
TR	Tropical nights – annual count of days when the daily T_{min} is above 20°	days year^{-1}
10p Tmin	10th percentile of daily T_{min}	°C
TNn	Annual minimum value of daily T_{min}	°C

The EM climate conditions are characterized by moderate air temperatures and changeable rainy weather during the cooler winter season and dry and stable hot weather during the summer. The region's climate is strongly affected by external forcing of both mid-latitude and tropical origins (Alpert *et al.,* 2005). Most of the annual precipitation takes place during a limited number of rainy days. The rainy events are typically associated with intrusions of cold air masses of North-European origin and penetration of warm humid masses originating from tropical Atlantic and/or equatorial regions of Eastern Africa and Arabian Sea (Krichak *et al.,* 2004, 2015; Ziv *et al.,* 2005; De Vries *et al.,* 2013). Topographical and coastal characteristics (with windward effects, gap winds, land-sea breezes, etc.) also influence the spatial distribution of climate characteristics in the region (Krichak *et al.,* 2010). The effects are especially notable in the mountainous and immediate coastal areas of the EM.

The quality of RCM results in the EM appears to be quite sensitive to the ability of the model to capture: (1) The role of long-term climate variations and especially those characterized by the frequency and intensity of the blocking situation in Europe often causing persistent heat waves and/or droughts in the EM (Fang *et al.,* 2008; Önol, 2012) and (2) The effects of teleconnections as well as the role of moist air mass transports from the tropics (Krichak *et al.,* 2014, 2015, 2016). The specific peculiarity of the EM regional climate resulting from the region's geographic location on the border between the mid-latitude and subtropical zones create additional constrains for using the RCM approach (Evans *et al.,* 2004; Krichak *et al.,* 2007). An important role of anomalously intense transports of moist air from the tropical and subtropical Atlantic and Indian Oceans in the occurrence of extreme precipitation events in the EM has been identified (Alpert *et al.,* 2005; Krichak *et al.,* 2015, 2016). According with these considerations, the evaluation of an RCM to represent the extremes is very relevant in the EM. It should be noted that Endris *et al.* (2016) have concluded that the relative contribution of teleconnection errors from boundary forcing is larger than the chosen RCM and its configuration. In other words, GCMs ability in simulating the boundary conditions for the RCM should also be evaluated before attempting a downscaling experiment. This was beyond the scope of this study. Nevertheless, this issue was partly addressed in a separate analysis (Gershtein *et al.*, 2015).

Extreme weather events have many aspects with essential influence on human life, economy, and ecosystems, especially in the EM (Ziv *et al.*, 2013; Kelley *et al.*, 2015). While monthly means provide useful information to detect slow climate change processes, an impact is often the result of short-term phenomena occurring well into the distribution tails of daily data (Zhang *et al.*, 2011). To gain a uniform perspective on observed changes in weather and climate extremes, an internationally coordinated core set of 27 indices for moderate temperature and precipitation extremes was defined by the Expert Team on Climate Change Detection and Indices (ETCCDI) (Klein-Tank *et al.*, 2009; Zhang *et al.*, 2011). These extreme indices find multiple applications in climate research due to their statistically robustness and a wide range of the climate covered. The indices considered in the present study, represent a subset of the standard ETCCDI ones. Eight precipitation and six temperature indices (Tables 1 and 2, respectively) have been selected from those widely used in the literature in the past (e.g. Samuels *et al.,* 2011; Smiatek *et al.,* 2011; Soares *et al.,* 2012; Domínguez *et al.*, 2013; Turco *et al.,* 2013; Zollo *et al.,* 2016). All the ETCCDI indices were calculated on a yearly basis and then averaged in order to obtain a climatological mean. On the contrary, percentiles were calculated from the distribution representing the whole period (Zollo *et al.,* 2016). It should be noted that as the summer dry season is from May to September, the Consecutive Dry Days (CDD) index over the EM

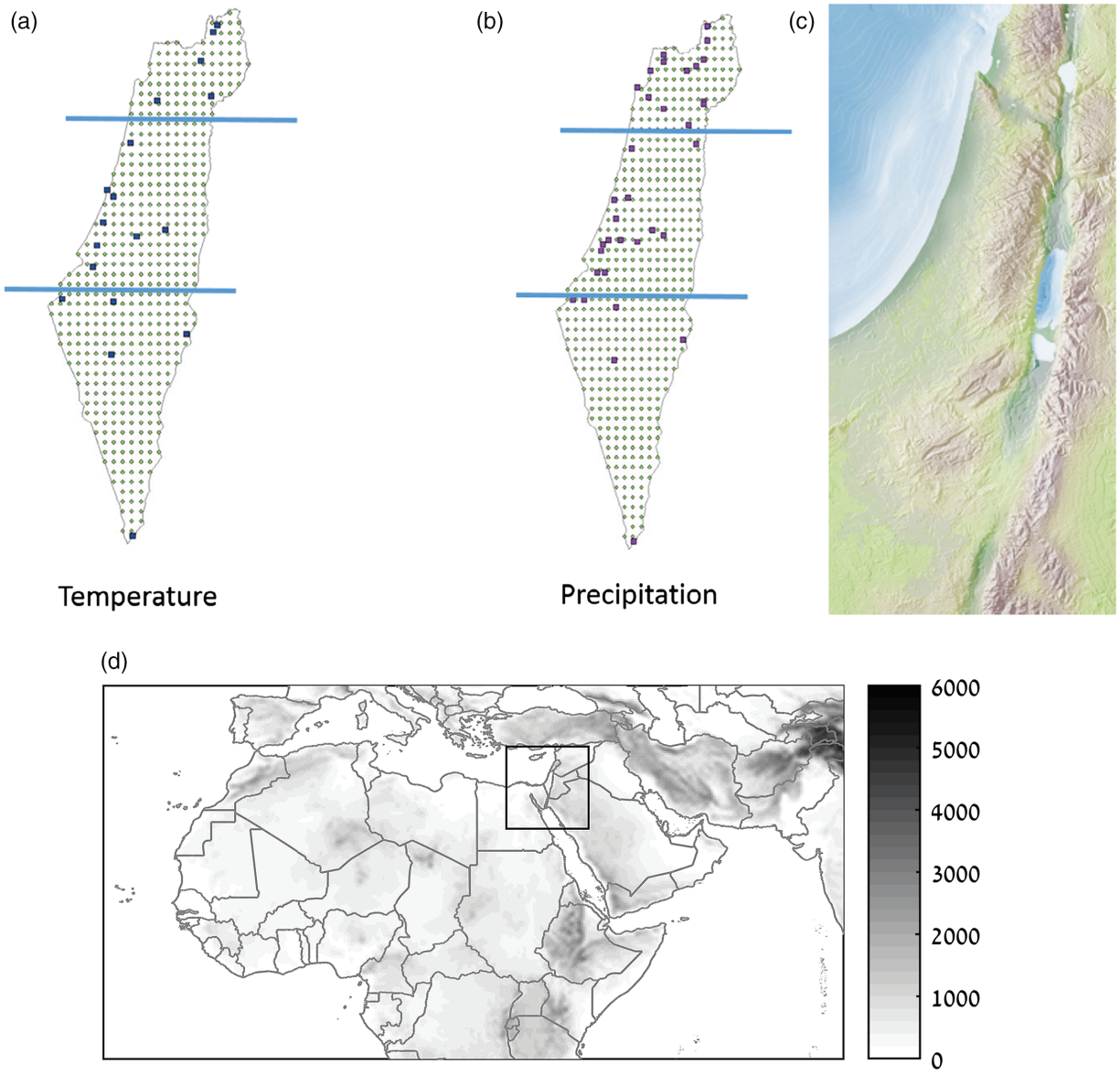

Figure 1. Distribution of available IMS station data for temperature (a) and precipitation (b), super-imposed over the COSMO-CLM ISR715 computational grid. (c) Topographic map of Israel. Dark areas indicate higher elevation. (d) The CORDEX-MENA domain with the Israel domain (ISR715) presented in a black rectangle. [Colour figure can be viewed at wileyonlinelibrary.com].

region represents the period between the last day of precipitation in spring and the first day in the autumn. On the other hand, observed rainy days present a more regular occurrence rate, so the Consecutive Wet Days (CWD) index represents wet spells during the winter.

The model domain used for the present analyses (MENA) is one of the domains suggested for the Coordinated Regional climate Downscaling Experiment (CORDEX) project (Giorgi *et al.,* 2009), endorsed by the World Climate Research Program (WCRP) and thus providing global coordination of Regional Climate Downscaling (RCD) for improved regional climate change adaptation and impact assessment. A set of common domains, encompassing the majority of the populated land areas worldwide have been defined within CORDEX.

The CORDEX-MENA domain (27 W–76 E, 7 S–45 N; Figure 1(d)), which includes a significant part of the tropical and mid-latitude Atlantic and Indian oceans, North Africa, southern Europe and the Arabian Peninsula, offers considerable advantages for assessing and understanding climate change over the region due to its larger size and complex topography, including highland areas. It is worth noting that the positioning of the western/eastern lateral boundary over the Atlantic and Arabian Sea, respectively, allows an accurate representation of the export of moist air masses to the Mediterranean region and the adequate representation of teleconnections in the boundaries.

The RCM used in this study is COSMO-CLM (Rockel *et al.*, 2008), which is the climate version of the three-dimensional, non-hydrostatic mesoscale weather forecast model COSMO (Steppeler *et al.*, 2003; Baldauf *et al.*, 2011), developed and operationally used by a consortium including the meteorological services of Germany, Switzerland, Italy, Greece, Romania, Poland, Russia and

Table 3. List of IMS precipitation (left) and temperature (right) stations.

Precipitation			Temperature		
Station number	Height (m)	Station name	Station number	Height (m)	Station name
110698	8	Akko	1540	15	En Hahoresh
311204	170	Ayyelet Hashahar	2008	15	Tel Aviv Sede Dov
251691	279	Beer Sheva	2523	31	Bet Dagan B
140801	55	Beer Tuveya	3080	50	Qevuzat Yavne
136580	55	Beerot Yizhaq	3502	95	Negba
246550	355	Beit Jimal	4642	936	Zefat Har Kenaan
230450	−40	Bet Hashitta	5501	50	Kefar Yehoshua
320500	−200	Deganya Alef	6771	810	Jerusalem Centre
250150	110	Dorot	7151	355	Beit Jimal
347702	22	Elat	7333	115	Dorot
210748	300	Elon	7850	279	Beer Sheva
131600	15	En Hahoresh	8206	475	Sede Boqer
138250	50	Gan Shelomo	8263	135	Dafna
120202	5	Haifa Port	8470	75	Kefar Blum
244730	810	Jerusalem Centre	9111	−200	Zemah
140850	125	Kefar Menahem	9571	−388	Sedom
320450	−170	Kinneret Kvuza	9974	22	Elat
144800	135	Magen	3891	110	Besor Farm
141150	70	Massuot Yizhaq			
310050	205	Mayan Barukh			
136650	20	Miqwe Yisel			
141746	85	Negba			
310600	75	Neot Mordekhay			
212600	430	Parod Gardosh			
243500	660	Qiryat Anavim			
250250	170	Ruhama			
220600	125	Sarid			
321800	−185	Sed Eliyyahu			
253000	475	Sede Boqer			
251550	100	Urim			
120750	25	Yagur			
211350	380	Yehiam			
211900	936	Zefat Har Kenaan			
337000	−388	Sedom			

Israel. A description of the main features of the model and of the configuration used were reported by Bucchignani *et al.* (2016a), in which different simulations were analysed in order to investigate the ability of the model to reproduce the average temperature and precipitation over the CORDEX-MENA domain.

Zollo *et al.* (2016) have evaluated the ability of the model to reproduce extreme precipitation and temperature indices over Italy. The precipitation indices displayed overestimations of the model over mountainous regions along with underestimations elsewhere. The temperature indices show underestimation for both maximum and minimum temperature indices.

The aim of this study is to investigate the ability of the model to represent the climate conditions in the EM with special emphasis on extreme climate indices.

2. Initial/verification data and setup of experiment

Two simulations have been performed over the CORDEX-MENA domain (Bucchignani *et al.*, 2016b), respectively, at spatial resolution of 0.44° (MNA44) and 0.22 (MNA22). The simulated period extended from January 1979 to December 2011. The optimized model configuration elaborated in Bucchignani *et al.* (2016a) has been used. Initial and boundary conditions were provided from ERA-Interim reanalysis (Dee *et al.,* 2011), characterized by horizontal resolution of ∼80 km. The computational domain includes a relaxation zone of at least 15 grid-points at each side. Moreover, a very high-resolution simulation over Israel (domain 28.01–39.45 E, 24.01–35.45 N; Figure 1(d)) at 0.0715° (about 8 km) nested into MNA22, has been performed for 1979–2011: this simulation is referred to as ISR715. The model configuration for ISR715 was optimized by means of a sensitivity analysis performed over the period 1979–1984. It includes the parameterization of albedo derived from MODIS data (Lawrence and Chase, 2007) and the NASA-GISS AOD distribution (Tegen *et al.,* 1997). Furthermore, it is characterized by a low value of the scaling factor of the laminar boundary layer for heat (rlam_heat = 0.1) (Bucchignani *et al.*, 2016a), which enhances the surface evaporation and increases precipitation amounts calculated in the model.

The model output for the three simulations in terms of average properties was validated against E-OBS and

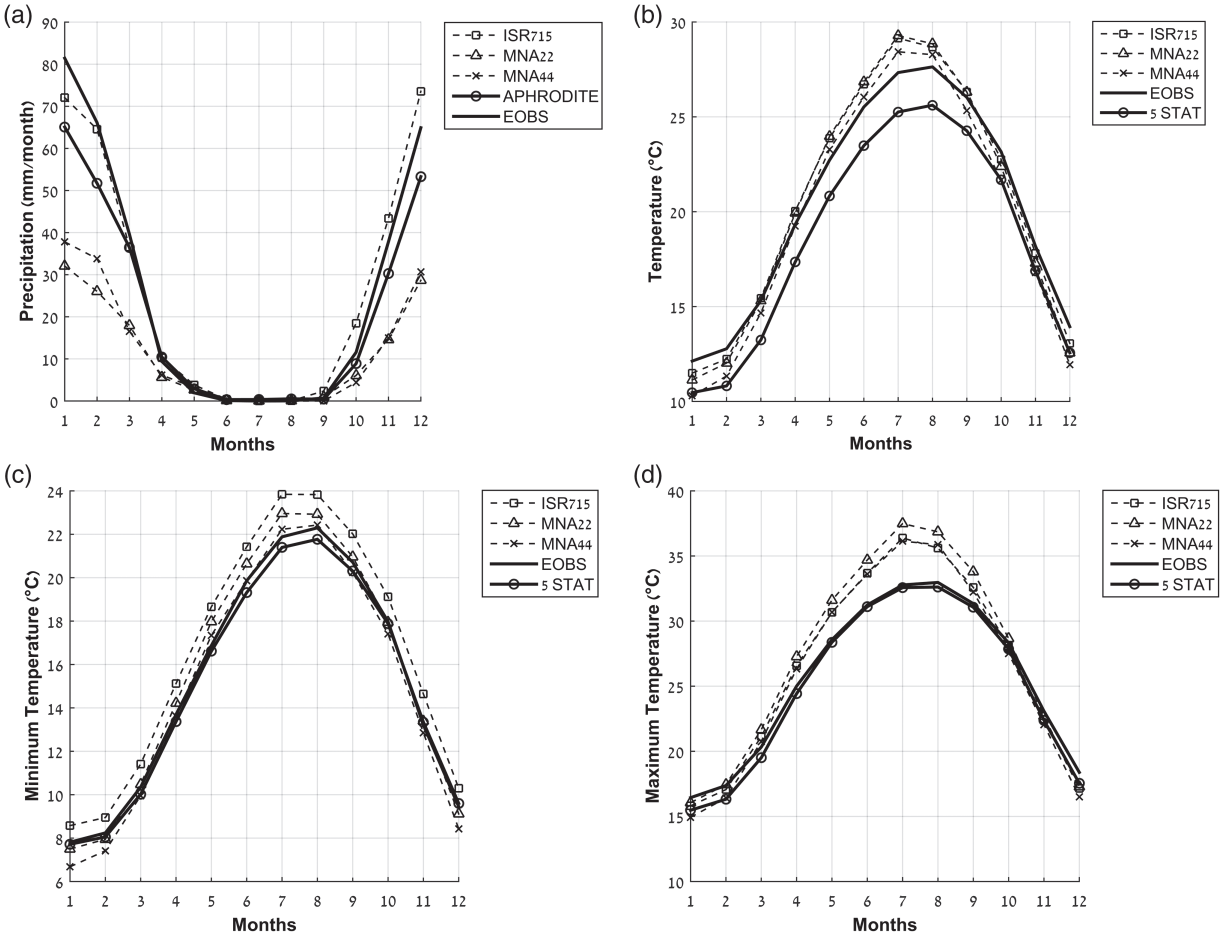

Figure 2. Annual cycle of monthly averaged: (a) precipitation (averaged for 1980–2007); (b) mean daily temperature (T_g, averaged for 1980–2011) (c) minimum daily temperature (T_n, averaged for 1980–2011) (d) maximum daily temperature (T_x, averaged for 1980–2011), for COSMO-CLM simulations with increasing resolution MNA44, MNA22, ISR715 and observations (E-OBS, APHRODITE and IMS 5 stations homogenized national average (5STAT)).

APHRODITE datasets. E-OBS from the EU-FP6 project ENSEMBLES (http://ensembles-eu.metoffice.com) (Haylock *et al.*, 2008) is a widely used gridded dataset of precipitation and temperature at 0.25° spatial resolution available for the period 1980–2011. It has been designed to provide the best estimate of grid box averages to enable direct comparison with RCMs (Tanarhte *et al.,* 2012). APHRODITE (Yatagai *et al.,* 2008, 2012), is a gridded dataset (28 km spatial resolution) characterized by daily values of precipitation for the period 1980–2007, over the EM region, whereas over Israel the database has a much higher spatial resolution (around 5 km). It is based on a dense network of rain gauges in the Middle East. It was shown that this data could serve as a good evaluating tool for climate models performance. In addition, when APHRODITE is compared with other gridded datasets (e.g. New *et al.*, 1999; Huffman *et al.*, 2001) it can demonstrate the effect of orography on precipitation (Yatagai *et al.*, 2008). The comparisons of model data (at the different resolutions) against gridded datasets for bias evaluation have been performed through a remapping of the model data onto the dataset grid using bilinear interpolation.

Model evaluation in terms of extreme events was performed against the Israel Meteorological Service (IMS) dataset. The daily IMS dataset includes 34 precipitation and 18 temperature stations, covering the period 1980–2011 (Table 3, https://ims.data.gov.il/). For each station, the nearest point in the model has been compared with the observational value. Figures 1(a)–(c) show the distribution of available IMS station locations for temperature and precipitation, superimposed on the ISR715 computational grid, along with a topographic map of the region for interpretation of the validation results shown in the next section.

The comparison of the mentioned indicators, evaluated from the simulated daily data, with those from observational datasets has been performed over the periods defined by data availability. In any case, the first year of the simulation (1979) has been removed, as the spin-up period is influenced by initial conditions, following the methodology already employed in other studies (e.g. Zollo *et al.,* 2016). Analysis against IMS dataset for extreme events has been conducted considering three sub-domains, namely north, centre and south Israel. According with Zollo *et al.* (2016) all indices were calculated on a yearly basis and then averaged in order to obtain a climatological mean. In contrast, percentiles values were calculated from distributions representing the

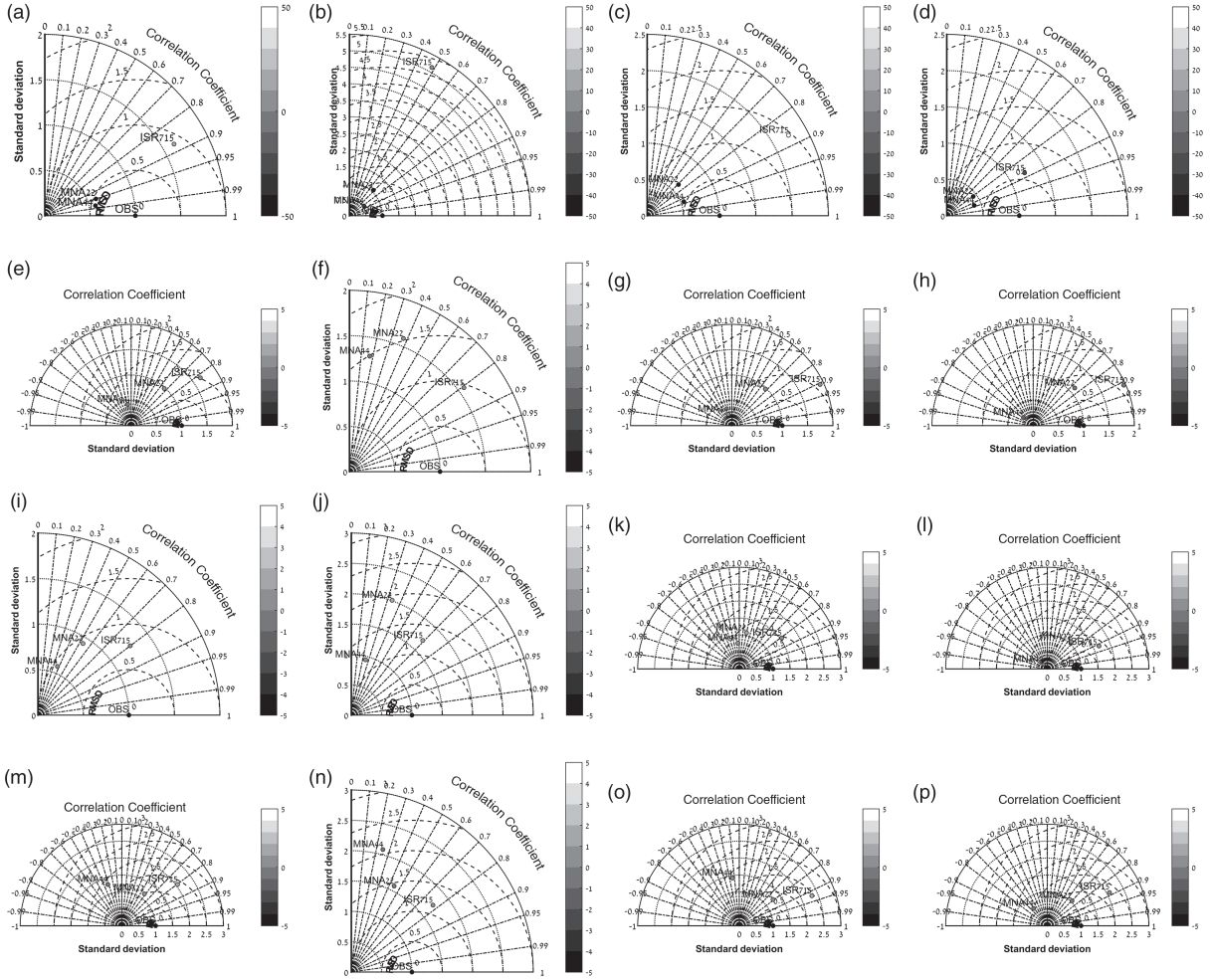

Figure 3. Taylor diagrams of (a–d) precipitation (1980–2007) (e–h) average temperature (T_g, 1980–2011) (i–l) maximum temperature (T_x, 1980–2011) (m–p) minimum temperature (T_n, 1980–2011). Columns from left to right are Israel and its subdomains namely north, centre and south, respectively, as defined in Figure 1.

whole period. Validation of the model data was performed considering standard verification measures (e.g. correlation coefficients, standard deviations, root mean square differences and the bias) in order to assess spatial agreement of climatological values between RCM output and observations.

3. Validation of results

3.1. Average properties of precipitation and temperature

Two-meter average temperature (T_g), minimum temperature (T_n), maximum temperature (T_x) and precipitation are the most basic climate variables. Even if extremes have a larger impact on society, a good representation of their average values is a precondition for in depth analysis.

In order to investigate the effects of increased resolution on the quality of the COSMO-CLM runs, the average annual values of precipitation T_g, T_n and T_x over Israel obtained with MNA44, MNA22, and ISR715 were compared with observations. Results are shown in the following order: (1) annual cycle over Israel domain (Figure 2); (2) Taylor diagrams for Israel and its subdomains (Figure 3); (3) probability distributions for a mountainous (Jerusalem) and a coastal plain (Negba) station (Figure 4). The analysis is presented from the larger temporal spatial resolution (annual, all of Israel) to the finer resolution (daily, station data).

Figure 2 shows the annual cycle of precipitation (Figure 2(a)), T_g, T_n and T_x (Figures 2(b)–(d), respectively), with respect to E-OBS, APHRODITE and IMS 'national average'. IMS 'national average' is based on five representing monthly homogenized temperature stations across Israel, with a long record (Yosef *et al.,* 2014): Jerusalem (urban, central mountains 810 m), Bet Jimal (rural, central hills 355 m), Zefat (forest, northern mountains 936 m), Negba (rural, southern coastal plain 95 m) and Eilat (desert, 22 m). Note that each dataset was evaluated on its native grid.

In the winter (DJF) season, the average bias between observations and ISR715 is about 10 mm month^{-1}, while the difference with MNA22 and MNA44 is in the range of 30–60 mm month^{-1} (Figure 2(a)). The improvement in simulating precipitation is not only related to spatial resolution but also to other variables such as model configuration and model physics, that in long-term precipitation climatology were found to be even more

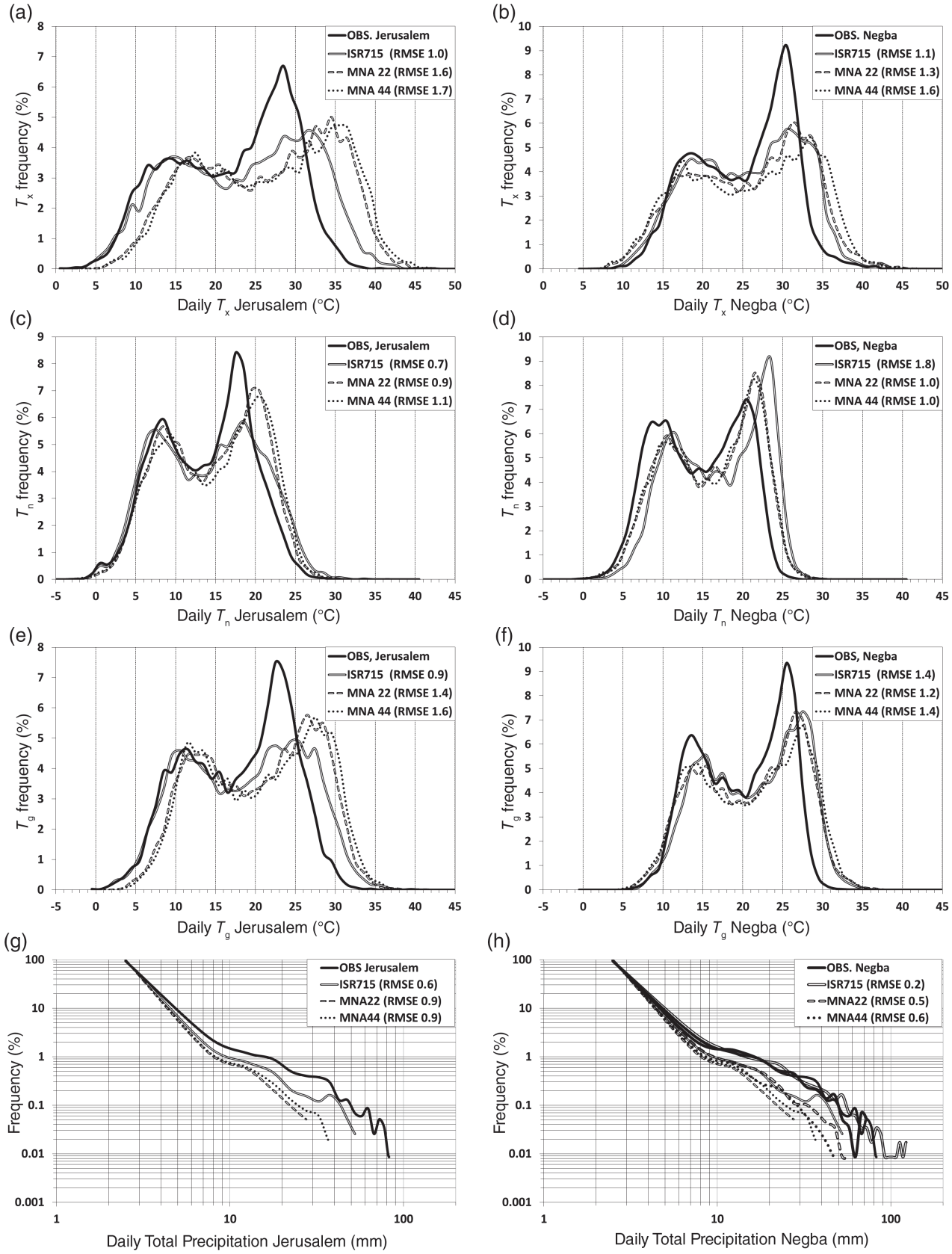

Figure 4. Jerusalem (left column) and Negba (right column) stations probability distributions for MNA44, MNA22, ISR715 and observations (OBS) of daily maximum temperature T_x (a, b), minimum temperature T_n (c, d), average temperature T_g (e, f) and precipitation (g, h).

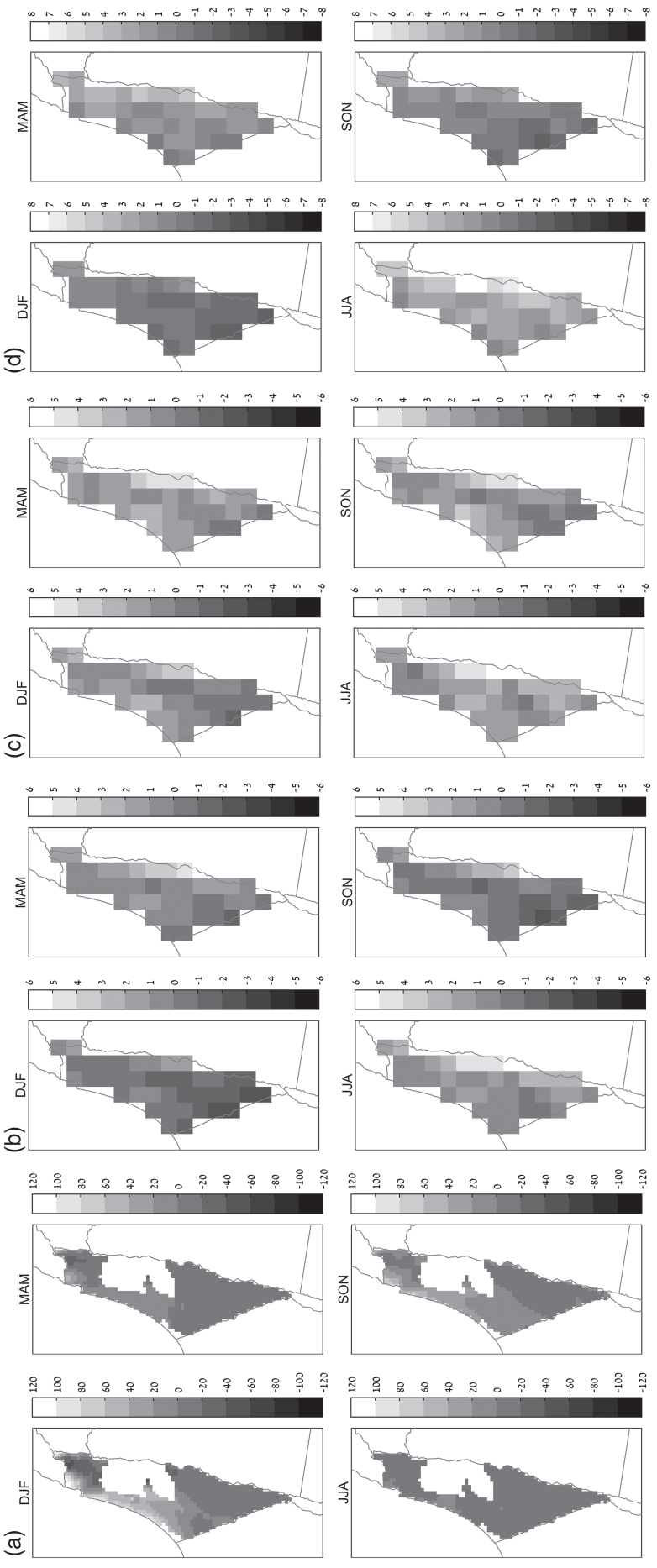

Figure 5. Seasonal bias of ISR715 precipitation (a), average temperature (T_g, b), minimum temperature (T_n, c) and maximum temperature (T_x, d) versus APHRODITE and E-OBS observation datasets.

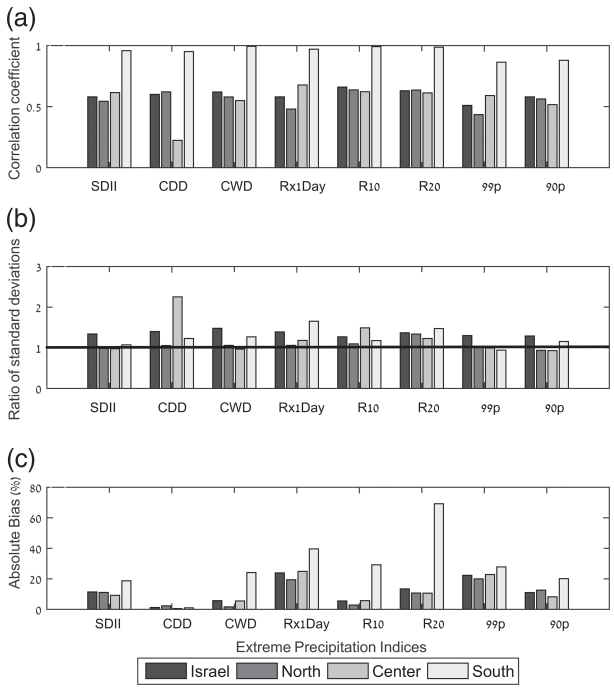

Figure 6. Overall error measures of COSMO-CLM (8 km) versus IMS dataset for precipitation indices (1980–2011): (a) correlation coefficients (b) ratio between modelled and observed standard deviation (c) percentage absolute bias. The values are shown for Israel and its subdomains namely north, centre and south as defined in Figure 1. The indices are defined in Table 1.

Table 4. Comparison of the COSMO-CLM run presented here and RegCM3-MM5 ensemble run over Israel (Samuels *et al.,* 2011).

Extreme Precipitation Index	COSMO-CLM bias 8-km resolution	RegCM3-MM5 ensemble bias 25-km resolution Samuels *et al.* (2011)
CWD (days year^{-1})	0.3 (5.4%)	−1 (−15%)
R10 (days year^{-1})	0.7 (4.3%)	0.83 (6%)
R20 (days year^{-1})	0.9 (12%)	1.67 (32%)

important (Cavicchia *et al.,* 2016). The MNA44 and MNA22 use the same model configuration, optimized over the whole MENA region at 0.44°. This is probably why MNA44 seems to simulate precipitation better than MNA22, during winter months. The low bias value of ISR715 winter precipitation represents a significant improvement with respect to earlier studies (e.g. Önol and Semazzi, 2009; Smiatek *et al.,* 2011; Bozkurt *et al.,* 2012), which displayed winter precipitation biases of $\sim 30-40$ mm month^{-1}. Improvement in temperature is also shown for the cold months, but a worsening of performance is observed for the warm months. Temperature at ground level is influenced by sea breeze, soil moisture, turbulent heat fluxes, and even the representation of vegetation parameters such as leaf area index (LAI), plant cover and root depth. These parameters might not be well represented in the warm/dry months as compared with the cold/wet months.

Figure 3 displays the Taylor diagrams of precipitation, T_g, T_x and T_n (rows from top to bottom, respectively) for Israel and its subdomains namely north, centre and south (columns from left to right, respectively) with respect to observations (APHRODITE for precipitation and E-OBS for temperature). As expected, all panels show that ISR715 exhibits greater variability than observations, due to the higher resolution. For temperature (Figures 3(e)–(p)) an improvement is generally shown for ISR715 compared with MNA44 and MNA22. For precipitation (Figures 3(a)–(d)) ISR715 shows an improvement in the bias, but does not show any improvement in correlation or Root Mean Square Difference (RMSD). The high-resolution model is probably punished in these verification measures because averaged spatial Taylor diagrams smooth out the extremes. It is shown that the correlations of high resolution runs improve as the size of the region is reduced, from all of Israel to the subdomains. Hence, the daily temperature and precipitation probability distributions for station data are displayed next.

Figure 4 presents the probability distributions of temperature and precipitation (observed and simulated) for Jerusalem and Negba stations. The left/right tails of the temperature distributions relates to winter/summer seasons, respectively. For T_x (Figures 4(a) and (b)) the left and right tails of the distributions for Negba/Jerusalem located on the coastal-plain/mountain-top, are better simulated by the higher resolution run (ISR715). In summer, a pronounced peak in the distribution is found in observations. All the three simulations do not correctly depict this peak. However, ISR715 is closest to observations. The EM summer maximum temperature is governed by the sea breeze circulation (Levi *et al.,* 2011). If the cool westerly winds are not properly simulated in the model due to the lack of resolution, then an overestimation would be simulated, as clearly shown. In addition, the overestimations are larger in summer than in winter because the modelled temperature is probably inside the temperature inversion layer. Furthermore, the difference between the real and modelled topographical heights is ∼10 m for Negba and ∼80 m for Jerusalem, therefore the overestimation related to this difference can be 0.05–0.1 °C for Negba and 0.4–0.8 °C for Jerusalem. Minimum temperatures are more susceptible to station location with respect to topography. Negba is more affected by this effect in comparison with the mountain top Jerusalem station (Figures 4(c) and (d)). Moreover, the temperature lapse rate at night is relatively moderate as compared with day time lapse rates, therefore the differences with observations are smaller than in T_x. The above mentioned effects on the distribution are smoothed out in average temperature (Figures 4(e) and (f)).

The precipitation probability distributions for Jerusalem and Negba (Figures 4(g) and (h), respectively) are presented in logarithmic scale to emphasize the distribution tail for extreme daily precipitation. For both stations, it is evident that the high resolution (ISR715) outperforms the coarser resolution simulations. For Negba, the daily precipitation is simulated well towards values of ∼90 mm day^{-1}, with overestimations in the extreme

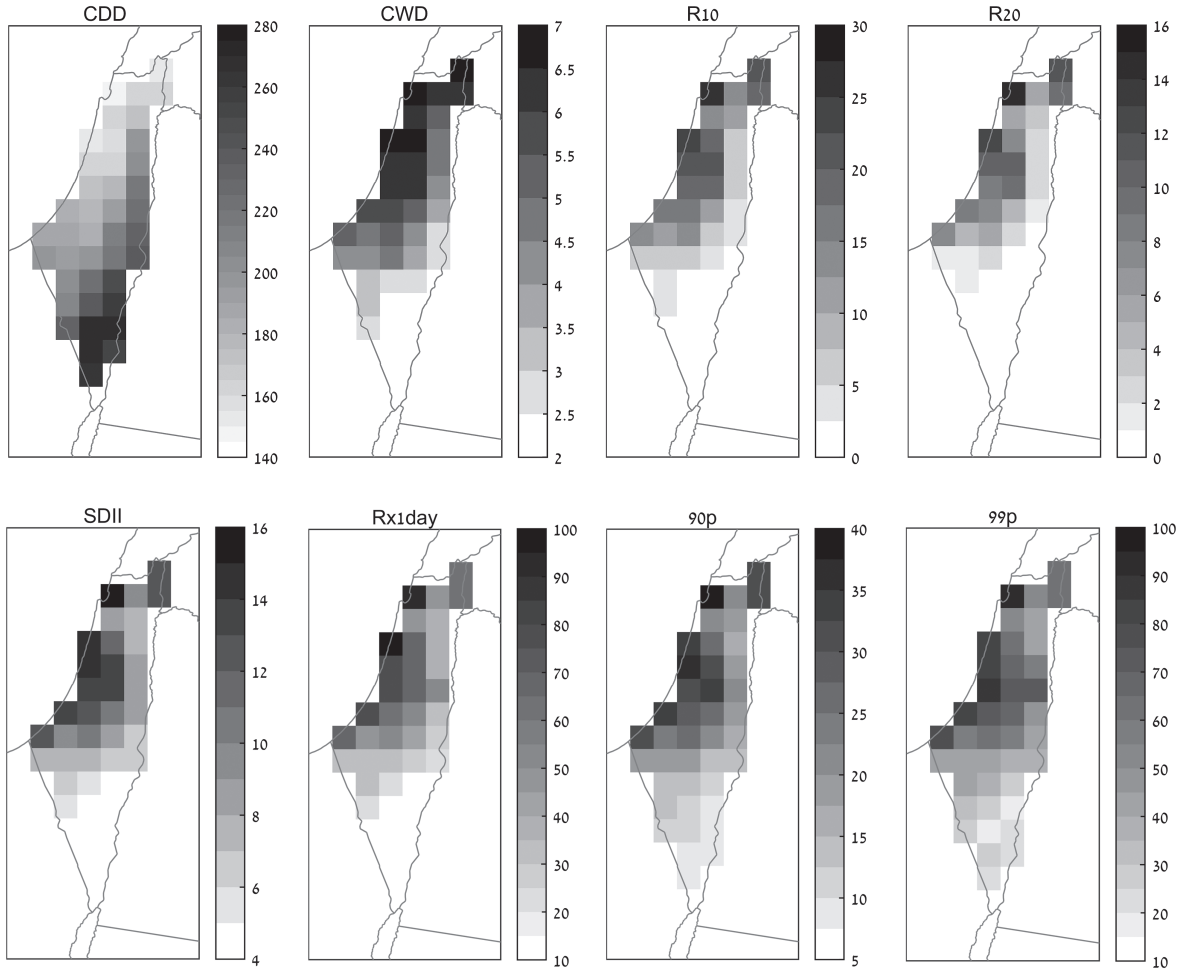

Figure 7. Climatology of COSMO-CLM (1980–2011) Extreme Precipitation Indices (EPI) based on day counts (top row) and measured in mm/day (bottom row) EPI are defined in Table 1.

precipitation. For Jerusalem, even the high resolution run is not yet enough to correctly portray the orographic effect. Nevertheless, the high resolution run is closer to observations with underestimations in the extreme precipitation.

Spatial patterns of seasonal precipitation, T_g, T_n and T_x bias values of ISR715 against APHRODITE 5 km (precipitation) and E-OBS 25 km (temperature) datasets are displayed in Figure 5. An east–west dipole of overestimations in the coastal plains and underestimations in the mountainous regions is found in seasonal precipitation (Figure 5(a)). The findings for seasonal temperature are shown in Figures 5(b)–(d). Overestimations are generally found for T_n (Figure 5(c)). For T_x, underestimations are found in winter and overestimations in summer (Figure 5(d)). The spatial patterns for seasonal precipitation and temperature in Figure 5 are consistent with the findings in Figure 4, discussed above.

3.2. Extreme precipitation indices (EPI)

Modelled extreme precipitation indices (EPI) have been compared with those obtained using the IMS observational dataset, in order to evaluate the capabilities of COSMO-CLM to simulate these indicators. Figure 6 displays the spatial correlation (Figure 6(a)), the ratio between standard deviations (Figure 6(b)) and the absolute bias (in %, Figure 6(c)) of model versus observations, for the whole country and for the subdomains, namely north, centre and south. In general, correlations are larger than 0.5 (Figure 6(a)) and the variability in modelled EPI is higher than in observations (Figure 6(b)). The model reveals a good capability in reproducing these indicators, with absolute bias for Israel EPI being ∼13% on average, comparable with Zollo *et al.* (2016) COSMO-CLM simulations over Italy. Furthermore, the simulations with COSMO-CLM show substantial improvement with respect to earlier studies (e.g. Samuels *et al.*, 2011), which used ensembles of RegCM3 and MM5 (25 km resolution) regional models (Table 4).

The maximum of daily precipitation (Rx1day) is the indicator affected by the largest percentage bias of 23.9% for the whole country (Figure 6(c)). Over Northern Israel, excellent performances are achieved, with average percentage of the absolute biases lower than 18% (Figure 6(c)). Over central Israel, the models performance is quite good. A large bias is observed in the south for Rx1day (∼40%) and 99p (22.8%). The absolute bias of the number of days with precipitation ≥20 mm

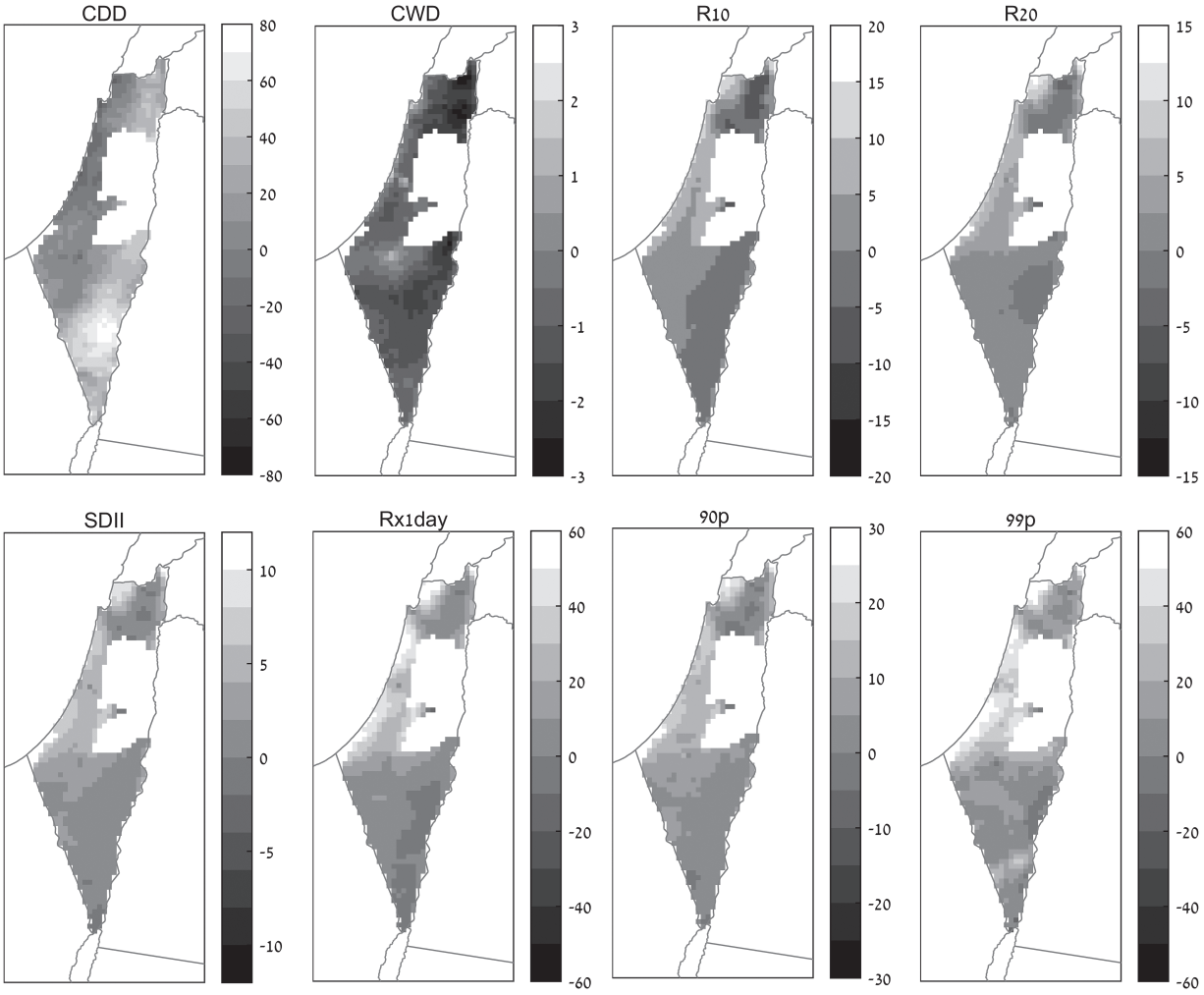

Figure 8. Annual bias of Extreme Precipitation Indices (EPI) based on day counts (top row) and measured in mm/day (bottom row) versus APHRODITE dataset (1980–2007). EPI are defined in Table 1.

(R20), for all regions, is reasonable (0.9 days year^{-1}), but the percentage error is high due to the low number of observed cases per days (∼7 days year^{-1}) exceeding the 20 mm threshold value (in the south, the observed value is even lower, 1.3 days year^{-1}). The analysis has been carried out also over southern Israel, which is characterized as a semi-arid to arid region. Absolute biases are generally good, the larger biases being recorded for Rx1day (9.5 mm day^{-1}) and 99p (10.1 mm day^{-1}). Nevertheless, in this region, a low number of observations leads to high percentage errors. A very good agreement is achieved for Consecutive Wet Days (CWD) index over Israel (5.7% bias).

Figure 7 displays the climatology of the eight EPI for the 1980–2011 period, as simulated by COSMO-CLM. The model is able to reproduce the EM north–south and west–east precipitation gradients. A spatial evaluation of EPI for the ISR715 run against APHRODITE dataset (at 5 km resolution) is presented in Figure 8.

It is shown that ISR715 displays underestimations for CWD, overestimations for R10 and R20 across the coastal plain, and underestimations across the central mountains (Figure 8). Overall, the EPI measured in millimeter per day (SDII, Rx1day, 90p, 99p) present overestimations. Note that the length of the dry season (CDD) is underestimated in the coastal plains and overestimated in the mountains (Figure 8). These findings are consistent with Figure 4, which shows overestimations in the coastal plains (Negba) and underestimations in the mountains (Jerusalem) for the extreme part of the precipitation distributions. These over/underestimations of extreme precipitation in the coastal-plains/mountains, respectively, are probably related to the exaggerated moisture availability in the cumulus parameterization, the low value of the scaling factor of the laminar boundary layer for heat (rlam_heat = 0.1) (Bucchignani *et al.,* 2016a), which enhances the surface evaporation and increases precipitation amounts calculated in the model and the still inadequate representation of topography in the 8 km resolution simulation.

3.3. Extreme temperature indices (ETI)

Modelled extreme temperature indices (ETI) have been compared with those obtained using the IMS observational dataset to evaluate the capabilities of COSMO-CLM

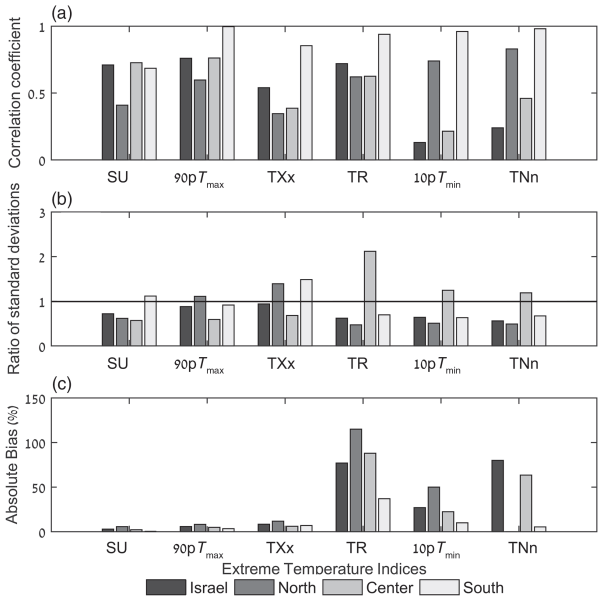

Figure 9. Same as Figure 6 but for temperature indices, which are defined in Table 2.

in simulating these indicators. Figure 9 contains the spatial correlation (Figure 9(a)), the ratio between standard deviations (SD, Figure 9(b)) and the absolute bias (in %, Figure 9(c)) of model versus observations, for the whole country and for the subdomains, namely north, centre and south. The analysis of the figure reveals that the indicators related to the maximum daily temperature (SU, 90pTmax, Txx) were well reproduced, portraying average bias of 5.7% (Figure 9(c)), average correlation of 0.67 (Figure 9(a)) and average STD of 0.85 (Figure 9(b)), for the whole country, comparable with values in Zollo *et al.* (2016).

The indices related to the minimum daily temperature (TR, 10pTmin, TNn) present a more complex picture (Figure 9) suggesting that the ability of ISR715 in reproducing IMS values are highly dependent on the station locations with respect to topography, as discussed in Section 3.1.

Figure 10 displays the climatology of the six ETI for the 1980–2011 period, as simulated by COSMO-CLM. The model is able to reproduce the EM north–south and west–east maximum temperature gradients. It is also shown that the model can reproduce the higher minimum temperatures on the Mediterranean coast, near the Dead-Sea and close to the Sea of Galilee.

Figure 11 presents a spatial evaluation of ETI bias for ISR715 run against E-OBS data set. A general overestimation of maximum temperature indices is reported. As discussed earlier with respect to Figure 4, maximum temperature in summer is mostly governed by the Mediterranean Sea breeze, and minimum temperatures are more susceptible to the station location with respect to topography. Therefore, if the model cannot reproduce the sea breeze then overestimations would be observed, and a more complex picture would be observed for minimum temperature indices, as shown.

4. Summary and conclusions

The main aim of this work was to evaluate the capabilities of COSMO-CLM in simulating extreme events over Israel. In particular, the skill to represent the climatology of a subset of ETCCDI indices for precipitation and temperature was investigated. A precondition to investigate the models ability in reproducing extremes is to evaluate whether the model can reproduce the basic average values.

It was shown that increased spatial resolution, from 50 to 8 km, improves the simulation of precipitation and temperature, due to better representation of topography and the location of land and sea in the model. The results display substantial improvement from earlier RCM studies in the region (e.g. Önol and Semazzi, 2009; Samuels *et al.,* 2011; Smiatek *et al.,* 2011; Bozkurt *et al.,* 2012). Nevertheless, some model deficiencies are still evident. This can be a result of either relatively sparse observation network in these regions, or the need of higher resolution ($\leq$ 3 km) models with convection permitting schemes.

Based on the results we can conclude that COSMO-CLM is capable of reproducing the EPI with an average absolute bias of ~13% for the whole region of Israel. In the northern part of Israel, where the Sea of Galilee is located, percentage biases drop below 10%. Over/underestimations of extreme precipitation were found in the coastal plains/mountains, respectively. These over/underestimations are probably related to the exaggerated moisture availability in the cumulus parameterization, and to the low value of the scaling factor of the laminar boundary layer for heat (rlam_heat = 0.1) (Bucchignani *et al.*, 2016a). This parameter enhances the surface evaporation and increases precipitation amounts calculated in the model. A further drawback is the still inadequate representation of topography in the 8 km resolution simulation.

The present results represent a substantial improvement from earlier studies in the region, and consistent with model simulations of EPI over Italy (Zollo *et al.,* 2016). The reproduction of extreme temperature indices is more complicated. The model relatively well reproduces the indices related to maximum temperatures, with percentage biases below 6%. The capability of the model in reproducing minimum temperatures is probably highly dependent on the location of observations with respect to topography.

The work described in the paper represents a first stage of a joint Italian –Israeli research effort focusing on assessing the impact of climate change on freshwater resources in the EM region, which is necessary for the identification of the socio-economic and environmental vulnerability caused by climate change impacts on water resources based on regional specificities.

The outcomes of the assessment aim to provide a common platform for addressing and responding to climate change impacts on freshwater resources in the EM, by serving as the basis for dialogue, priority setting and policy formulation on climate change adaptation at the

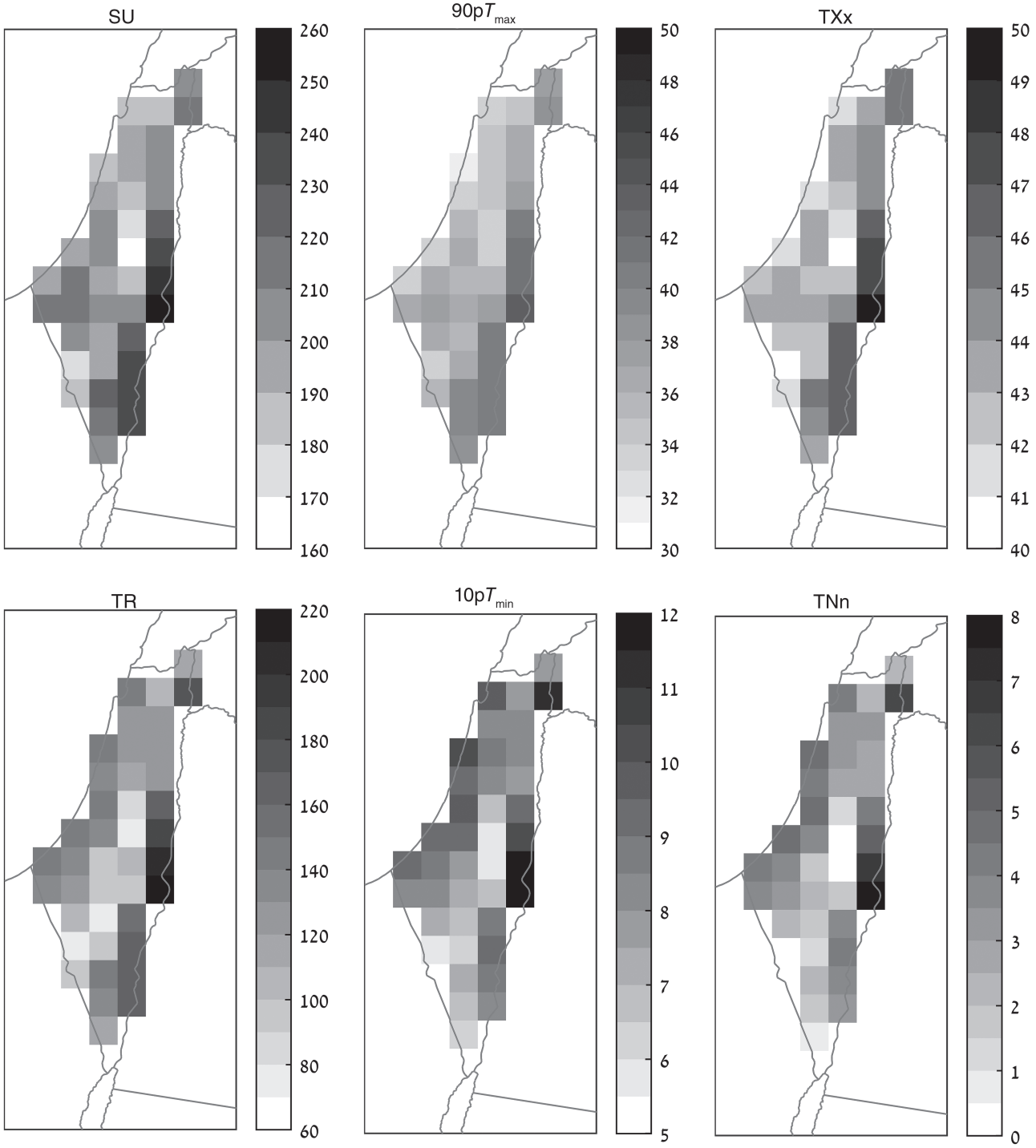

Figure 10. Same as Figure 7 but for Extreme Temperature Indices (ETI). ETI related to maximum temperature are given in the top row and ETI related to minimum temperature are given in the bottom row.

regional level. These aims are in line with an international research effort initiated by the Swedish International Development Cooperation Agency (SIDA), within the framework of the Regional Initiative for the Assessment of the Impact of Climate Change on Water Resources and Socio-Economic Vulnerability in the Arab Region (RICCAR).

Earlier results of RCM simulations have projected a high level of probability for a notable regional increase mean annual temperatures and decrease in the mean annual rainfall amount (Alpert *et al.,* 2008; Mariotti *et al.,* 2008; Önol *et al.,* 2014; Tanarhte *et al.*, 2015; Lelieveld *et al.,* 2016). Some of the most worrisome future impacts of climate change in the region are expected to be associated with shifts to extremes in frequency and intensity of precipitation events, specifically floods. The fact has great importance because the extremes can have devastating impacts at the local level. Future changes in precipitation and

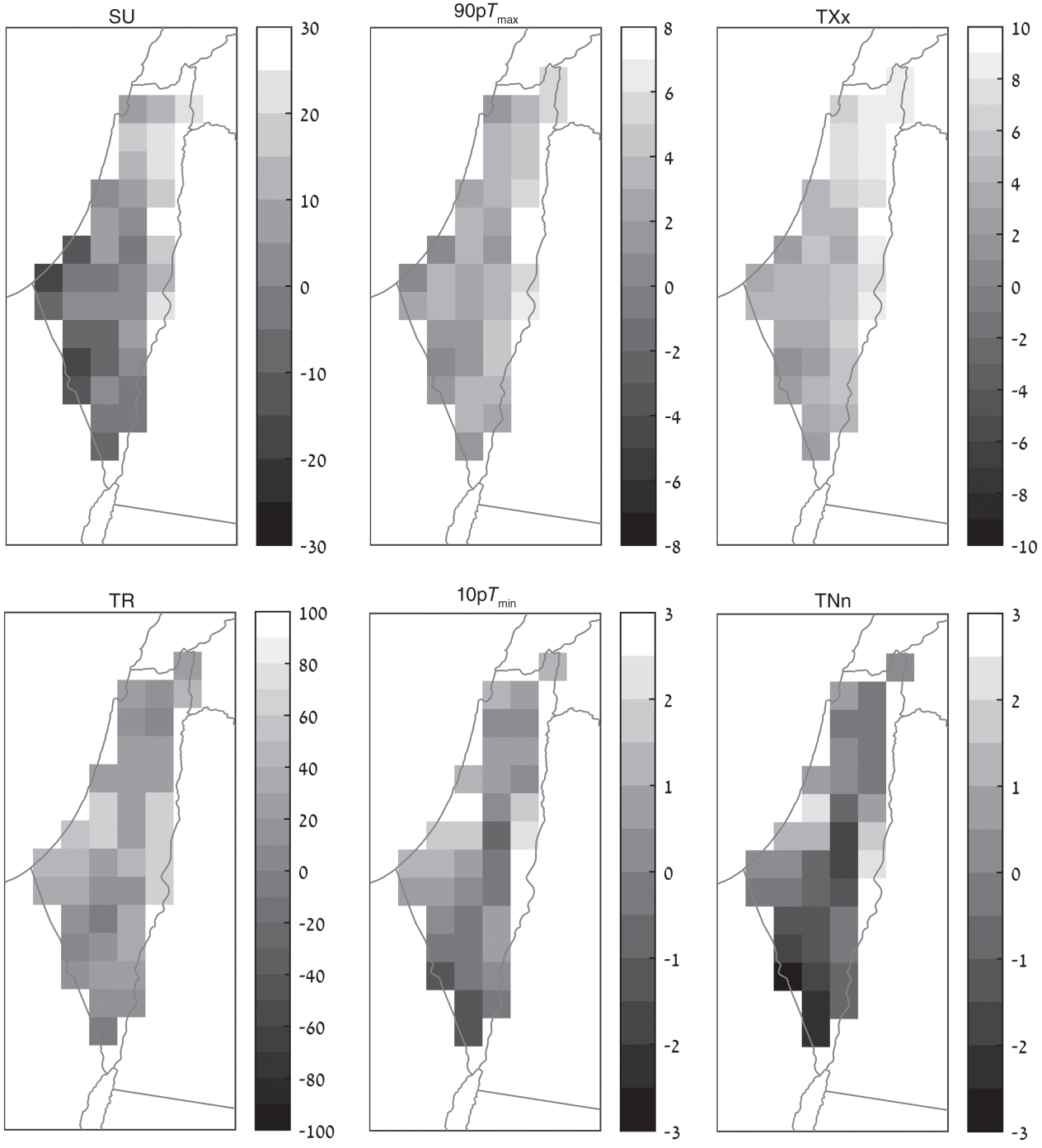

Figure 11. Same as Figure 8 but for Extreme Temperature Indices (ETI). ETI related to maximum temperature are given in the top row and ETI related to minimum temperature are given in the bottom row. The bias was calculated with respect to E-OBS dataset (1980–2011).

temperature extremes in the region are currently addressed in a complementary study.

Acknowledgements

This work was performed within the framework of the GEMINA project, funded by the Italian Ministry of Education, University and Research and the Italian Ministry of the Environment, Land and Sea. It was also supported by the Ministry Of Science and Technology (MOST) of the state of Israel, by the Tel-Aviv University (TAU) President and Mintz foundation and by the Porter School of Environmental Studies at TAU. The German Helmholtz Association is gratefully acknowledged for partly funding this project within the Virtual Institute DESERVE (Dead Sea Research Venue) under contract number VH-VI-527. We would like to thank the anonymous reviewers for their valuable time and useful contributions. The inputs suggested by the reviewers definitely helped improve this manuscript.

References

Alpert P, Price C, Krichak SO, Ziv B, Saaroni H, Osetinsky I, Barkan J, Kishcha P. 2005. Tropical tele-connections to the Mediterranean climate and weather. *Adv. Geosci.* **2**: 157–160. https://doi.org/10.5194/adgeo-2-157-2005.

Alpert P, Krichak SO, Shafir H, Haim D, Osetinsky I. 2008. Climatic trends to extremes employing regional modeling and statistical interpretation over the E. Mediterranean. *Global Planet. Change* **63**: 163–170. https://doi.org/10.1016/j.gloplacha.2008.03.003.

Baldauf M, Seifert A, Förstner J, Majewski D, Raschendorfer M, Reinhardt T. 2011. Operational convective-scale numerical weather prediction with the COSMO model: description and sensitivities. *Mon. Weather Rev.* **139**: 3887–3905. https://doi.org/10.1175/MWR-D-10-05013.1.

Bozkurt D, Turukonglu U, Lutfi Sen O, Önol B, Dalfes HN. 2012. Downscaled simulations of the ECHAM5, CCSM3 and HadCM3 global models for the Eastern Mediterranean–Black Sea region: evaluation of the reference period. *Clim. Dyn.* **39**: 207–225. https://doi.org/10.1007/s00382-011-1187-x.

Bucchignani E, Mercogliano P, Rianna G, Panitz HJ. 2016a. Analysis of ERA-Interim driven COSMO-CLM simulations over Middle East – North Africa domain at different spatial resolutions. *Int. J. Climatol.* **36**(9): 3346–3369. https://doi.org/10.1002/joc.4559.

Bucchignani E, Cattaneo L, Panitz HJ, Mercogliano P. 2016b. Sensitivity analysis with the regional climate model COSMO-CLM over the CORDEX-MENA domain. *Meteorol. Atmos. Phys.* **128**(1): 73–95. https://doi.org/10.1007/s00703-015-0403-3.

Cavicchia L, Scoccimarro E, Gualdi S, Marson P, Ahrens B, Berthou S, Conte D, Dell'Aquila A, Drobinski P, Djurdjevic V, Dubois C, Gallardo C, Li L, Oddo P, Sanna A, Torma C. 2016. Mediterranean extreme precipitation: a multi-model assessment. *Clim. Dyn.* https://doi.org/10.1007/s00382-016-3245-x.

Chan SC, Kendon EJ, Fowler HJ, Blenkinsop S, Ferro CAT, Stephenson DB. 2013. Does increasing the spatial resolution of a regional climate model improve the simulated daily precipitation? *Clim. Dyn.* **41**(5–6): 1475–1495. https://doi.org/10.1007/s00382-012-1568-9.

De Vries AJ, Tyrlis E, Edry D, Krichak SO, Steil B, Lelieveld J. 2013. Extreme precipitation events in the Middle-East: dynamics of the Red Sea Trough. *J. Geophys. Res.-Atmos.* **118**: 7087–7108. https://doi.org/10.1002/jgrd.50569.

Dee DP, Uppala SM, Simmons AJ, Berrisford P, Poli P, Kobayashi S, Andrae U, Balmaseda MA, Balsamo G, Bauer P, Bechtold P, Beljaars ACM, van den Berg L, Bidlot J, Bormann N, Delsol C, Dragani R, Fuentes M, Geer AJ, Haimberger L, Healy SB, Hersbach H, Hólm EV, Isaksen L, Kållberg P, Köhler M, Matricardi M, McNally AP, Monge-Sanz BM, Morcrette JJ, Park BK, Peubey C, de Rosnay P, Tavolato C, Thépaut JN, Vitart F. 2011. The ERA-Interim reanalysis: configuration and performance of the data assimilation system. *Q. J. R. Meteorol. Soc.* **137**(656): 553–597. https://doi.org/10.1002/qj.828.

Domínguez M, Romera R, Sánchez E, Fita L, Fernández J, Jiménez-Guerrero P, Montávez JP, Cabos WD, Liguori G, Gaertner MA. 2013. Present-climate precipitation and temperature extremes over Spain from a set of high resolution RCMs. *Clim. Res.* **58**: 149–164. https://doi.org/10.3354/cr01186.

Endris HS, Lennard C, Hewitson B, Dossio A, Nikulin G, Panitz HJ. 2016. Teleconnection responses in multi-GCM driven CORDEX RCMs over Eastern Africa. *Clim. Dyn.* **46**: 2821–2046. https://doi.org/10.1007/s00382-015-2734-7.

Evans JP, Smith RB, Oglesby RJ. 2004. Middle East climate simulation and dominant precipitation processes. *Int. J. Climatol.* **24**(13): 1671–1694. https://doi.org/10.1002/joc.1084.

Fang X, Wang A, Fong SK, Lin W, Liu J. 2008. Changes of reanalysis-derived Northern Hemisphere summer warm extreme indices during 1948–2006 and links with climate variability. *Global Planet. Change* **63**: 67–78. https://doi.org/10.1016/j.gloplacha.2008.06.003.

García-Cueto OR, Santillán-Soto N. 2012. Modeling extreme climate events: two case studies in Mexico. In *Climate Models*, Druyan L (ed). InTech: Rijeka, Croatia, 137–160. https://doi.org/10.5772/31634.

Gershtein G, Krichak SO, Levi Y. 2015. Comparative evaluation of climate simulation results with COSMO-CLM under the frameworks of Med-CORDEX and CORDEX-MENA COSMO/CLM/ART user seminar, Poster, 2–6 March 2015, DWD, Offenbach, Germany, https://doi.org/10.1515/dmdi-2014-0037.

Giorgi F, Jones C, Asrar GR. 2009. Addressing climate information needs at the regional level: the CORDEX framework. *WMO Bull.* **58**: 175.

Haylock MR, Hofstra N, Klein Tank AMG, Klok EJ, Jones PD, New M. 2008. A European daily high-resolution gridded dataset of surface temperature and precipitation. *J. Geophys. Res.-Atmos.* **113**: D20119. https://doi.org/10.1029/2008JD10201.

Huffman GJ, Adler RF, Morrissey MM, Bolvin DT, Curtis S, Joyce R, McGavock B, Susskind J. 2001. Global precipitation at one-degree daily resolution from multi-satellite observations. *J. Hydrometeorol.* **2**(1): 36–50. https://doi.org/10.1175/1525-7541(2001)002<0036:GPAODD>2.0.CO;2.

Kelley CP, Mohtadi S, Cane MA, Seager R, Kushnir Y. 2015. Climate change in the Fertile Crescent and implications of the recent Syrian drought. *Proc. Natl. Acad. Sci. U.S.A.* **112**(11): 3241–3246. https://doi.org/10.1073/pnas.1421533112.

Klein-Tank A. M. G, Zwiers F. W, Zhang X. 2009. Guidelines on analysis of extremes in a changing climate in support of informed decisions for adaptation. Climate data and monitoring, WCDMP-no. 72, WMO-TD no. 1500. Geneva, Switzerland.

Krichak SO, Alpert P, Dayan M. 2004. The role of atmospheric processes associated with Hurricane Olga in the December 2001 floods in Israel. *J. Hydrometeorol.* **5**: 1259–1270. https://doi.org/10.1175/JHM-399.1.

Krichak SO, Alpert P, Bassat K, Kunin P. 2007. The surface climatology of the eastern Mediterranean region obtained in a three-member ensemble climate change simulation experiment. *Adv. Geosci.* **12**: 67–80. https://doi.org/10.5194/adgeo-12-67-2007.

Krichak SO, Alpert P, Kunin P. 2010. Numerical simulation of seasonal distribution of precipitation over the eastern Mediterranean with a RCM. *Clim. Dyn.* **34**(1): 47–59. https://doi.org/10.1007/s00382-009-0649-x.

Krichak SO, Breitgard JS, Gualdi S, Feldstein SB. 2014. Teleconnection extreme precipitation relationships over the Mediterranean region. *Theor. Appl. Climatol.* **117**: 679–692. https://doi.org/10.1007/s00704-013-1036-4.

Krichak SO, Barkan J, Breitgard JS, Gualdi S, Feldstein SB. 2015. The role of the export of tropical moisture into midlatitudes for extreme precipitation events in the Eastern Mediterranean region. *Theor. Appl. Climatol.* **121**: 499–515. https://doi.org/10.1007/s00704-014-1244-6.

Krichak SO, Feldstein SB, Alpert P, Gualdi S, Scoccimaro E, Yano JI. 2016. Discussing the role of tropical and subtropical moisture sources in extreme precipitation events in the Mediterranean region from a climate change perspective. *Nat. Hazards Earth Syst. Sci.* **16**: 269–285. https://doi.org/10.5194/nhess-16-269-2016.

Laurent L, Casado A, Congedi L, Dell'Aquila A, Dubois C, Elizalde A, Hévéder BL, Lionello P, Sevault F, Somot S, Ruti P, Zampieri M. 2012. Modeling of the Mediterranean climate system. In *The Climate of the Mediterranean Region: From the Past to the Future*, Lionello P (ed). Elsevier: London, England, 419–448.

Lawrence PJ, Chase TN. 2007. Representing a new MODIS consistent land surface in the community land model (CLM 3.0). *J. Geophys. Res.* **112**(G1): G01023. https://doi.org/10.1029/2006JG000168.

Lelieveld J, Proestos Y, Hadjinicolaou P, Zittis G. 2016. Strongly increasing heat extremes in the Middle East and North Africa (MENA) in the 21st century. *Clim. Change* **137**(1–2): 245–260. https://doi.org/10.1007/s10584-016-1665-6.

Levi Y, Shilo E, Setter I. 2011. Climatology of a summer coastal boundary layer with 1290-MHz wind profiler radar and a WRF simulation. *J. Appl. Meteorol. Climatol.* **50**(9): 1815–1826. https://doi.org/10.1175/2011JAMC2598.1.

Lionello P, Abrantes F, Gacic M, Planton S, Trigo R, Ulbrich U. 2014. The climate of the Mediterranean region: research progress and climate change impacts. *Reg. Environ. Change* **14**: 1679–1684. https://doi.org/10.1007/s10113-014-0666-0.

Mariotti A, Zeng Z, Yoon JH, Artale V, Navarra A, Alpert P, Li LZX. 2008. Mediterranean water cycle changes: transition to drier 21st century conditions in observations and CMIP3 simulations. *Environ. Res. Lett.* **3**: 044001. https://doi.org/10.1088/1748-9326/3/4/044001.

New MG, Hulme M, Jones PD. 1999. Representing twentieth century space-time climate variability. Part I: development of a 1961–90 mean monthly terrestrial climatology. *J. Clim.* **12**: 829–856. https://doi.org/10.1175/1520-0442(1999)012<0829:RTCSTC>2.0.CO;2.

Önol B. 2012. Effects of coastal topography on climate: high-resolution simulation with a regional climate model. *Clim. Res.* **52**: 159–174. https://doi.org/10.3354/cr01077.

Önol B, Semazzi FHM. 2009. Regionalization of climate change simulations over the eastern Mediterranean. *J. Clim.* **22**(618): 1944–1961. https://doi.org/10.1175/2008JCLI1807.1.

Önol B, Bozkurt D, Turuncoglu UU, Lutfi Sen O, Dulfes HN. 2014. Evaluation of the twenty-first century RCM simulations driven by multiple

GCMs over the Eastern Mediterranean–Black Sea region. *Clim. Dyn.* **42**: 1949–1965. https://doi.org/10.1007/s00382-013-1966-7.

Rockel B, Will A, Hense A. 2008. The regional Climate Model COSMO-CLM (CCLM). *Meteorol. Z.* **17**: 347–348. https://doi.org/10.1127/0941-2948/2008/0309.

Samuels R, Smiatek G, Krichak S, Kunstmann H, Alpert P. 2011. Extreme value indicators in highly resolved climate change simulations for the Jordan River area. *J. Geophys. Res.* **116**: D24123. https://doi.org/10.1029/2011JD016322.

Smiatek G, Kunstmann H, Heckl A. 2011. High resolution climate change simulations for the Jordan River area. *J. Geophys. Res.* **116**: D16111. https://doi.org/10.1029/2010JD015313.

Soares PMM, Cardoso RM, Miranda PMA, Viterbo P, Belo-Pereira M. 2012. Assessment of the ENSEMBLES regional climate models in the representation of precipitation variability and extremes over Portugal. *J. Geophys. Res.* **117**: D07114. https://doi.org/10.1029/2011JD016768.

Steppeler J, Doms G, Schättler U, Bitzer HW, Gassmann A, Damrath A, Gregoric G. 2003. Meso-gamma scale forecasts using the non-hydrostatic model LM. *Meteorol. Atmos. Phys.* **82**: 75–96. https://doi.org/10.1007/s00703-001-0592-9.

Tanarhte M, Hadjinicolaou P, Lelieveld J. 2012. Intercomparison of temperature and precipitation data sets based on observations in the Mediterranean and the Middle East. *J. Geophys. Res.* **117**: D12102. https://doi.org/10.1029/2011JD017293.

Tanarhte M, Hadjinicolaou P, Lelieveld J. 2015. Heat wave characteristics in the eastern Mediterranean and Middle East using extreme value theory. *Clim. Res.* **63**: 99–113. https://doi.org/10.3354/cr01285.

Tegen I, Hollrig P, Chin M, Fung I, Jacob D, Penner J. 1997. Contribution of different aerosol species to the global aerosol extinction optical thickness: estimates from model results. *J. Geophys. Res.* **102**: 895–915. https://doi.org/10.1029/97JD01,864.

Toreti A, Naveau P. 2015. On the evaluation of climate model simulated precipitation extremes. *Environ. Res. Lett.* **10**: 014012.

Turco M, Zollo AL, Ronchi C, De Luigi C, Mercogliano P. 2013. Assessing gridded observations for daily precipitation extremes in the Alps with a focus on northwest Italy. *Nat. Hazards Earth Syst. Sci.* **13**: 1457–1468. https://doi.org/10.5194/nhess-13-1457-2013.

Yatagai A, Alpert P, Xie P. 2008. Development of a daily gridded precipitation data set for the Middle East. *Adv. Geosci.* **12**: 1–6.

Yatagai A, Kamiguchi K, Arakawa O, Hamada A, Yasutomi N, Kitoh A. 2012. APHRODITE: constructing a long-term daily gridded precipitation dataset for Asia based on a dense network of rain gauges. *Bull. Am. Meteorol. Soc.* **93**: 1401–1415. https://doi.org/10.1175/BAMS-D-11-00122.1.

Yosef Y, Osetinsky-Tzidaki I, Furshpan A. 2014. Homogenization of monthly temperature series in Israel – an integrated approach for optimal break-points detection. In *Proceedings of the 8th Seminar for Homogenization and Quality Control in Climatological Databases*. WCDMP-No. 84, 12–16 May 2014, Budapest, Hungary, WMO.

Zhang X, Alexander L, Hegerl C, Jones P, Tank AK, Peterson TC, Trewin B, Zwiers FW. 2011. Indices for monitoring changes in extremes based on daily temperature and precipitation data. *Clim. Change* **2**: 851–870.

Ziv B, Saaroni H, Baharad A, Yekutieli D, Alpert P. 2005. Indications for aggravation in summer heat conditions over the Mediterranean Basin. *Geophys. Res. Lett.* **32**: L12706. https://doi.org/10.1029/2005GL022796.

Ziv B, Saaroni H, Pargament R, Harpaz T, Alpert P. 2013. Trends in the rainfall regime over Israel, 1975-2010, and their relationship to large-scale variability. *Reg. Environ. Change* **13**: 1751–1764. https://doi.org/10.1007/s10113-013-0414-x.

Zollo AL, Rillo V, Buchignani E, Montesarchio M, Mercogliano P. 2016. Extreme temperature and precipitation events over Italy: assessment with high-resolution simulations with COSMO-CLM and future scenarios. *Int. J. Climatol.* **36**(2): 987–1005. https://doi.org/10.1002/joc.4401.

